NEOPLASIA
www.neoplasia.com

Volume 21 Number 2 February 2019 pp. 185–196 185

Tumor Initiation Capacity and Therapy Resistance Are Differential Features of EMT-Related Subpopulations in the NSCLC Cell Line A549[1]

Colin Charles Tièche[*,†], Yanyun Gao[*,†,2], Elias Daniel Bührer[‡,2], Nina Hobi[§], Sabina Anna Berezowska[¶], Kurt Wyler[#], Laurène Froment[*,†], Stefan Weis[**], Ren-Wang Peng[*,†], Rémy Bruggmann[#], Primo Schär[**], Michael Alex Amrein[‡], Sean Ralph Robert Hall[*,†], Patrick Dorn[*,†], Gregor Kocher[*,†], Carsten Riether[‡], Adrian Ochsenbein[‡], Ralph Alexander Schmid[*,†] and Thomas Michael Marti[*,†]

[*]Department of General Thoracic Surgery, Inselspital, Bern University Hospital, University of Bern, Switzerland; [†]Department of BioMedical Research (DBMR), University of Bern, Switzerland; [‡]Department of Medical Oncology, Inselspital, Bern University Hospital, University of Bern, Switzerland; [§]ARTORG Center for Biomedical Engineering Research, Organs-on-Chip Technologies, University of Bern, Switzerland, Institute of General Physiology, University of Ulm, Germany; [¶]Institute of Pathology, University of Bern, Switzerland; [#]Interfaculty Bioinformatics Unit and Swiss Institute of Bioinformatics, University of Bern, Switzerland; [**]Department of Biomedicine, University of Basel, Switzerland

Abstract

Cell lines are essential tools to standardize and compare experimental findings in basic and translational cancer research. The current dogma states that cancer stem cells feature an increased tumor initiation capacity and are also chemoresistant. Here, we identified and comprehensively characterized three morphologically distinct cellular subtypes in the non–small cell lung cancer cell line A549 and challenge the current cancer stem cell dogma. Subtype-specific cellular morphology is maintained during short-term culturing, resulting in the formation of holoclonal, meroclonal, and paraclonal colonies. A549 holoclone cells were characterized by an epithelial and stem-like phenotype, paraclone cells featured a mesenchymal phenotype, whereas meroclone cells were phenotypically intermediate. Cell-surface marker expression of subpopulations changed over time, indicating an active epithelial-to-mesenchymal transition (EMT), *in vitro* and *in vivo*. EMT has been associated with the overexpression of the immunomodulators PD-L1 and PD-L2, which were 37- and 235-fold overexpressed in para- versus holoclone cells, respectively. We found that DNA methylation is involved in epigenetic regulation of marker expression. Holoclone cells were extremely sensitive to cisplatin and radiotherapy *in vitro*, whereas paraclone cells were highly resistant. However, inhibition of the receptor tyrosine kinase AXL, whose expression is associated

Abbreviations: EMT, epithelial-to-mesenchymal transition; NSCLC, non–small cell lung cancers; CSCs, cancer stem cells; hybrid-E/M, hybrid epithelial/mesenchymal; GOseq, KEGG pathway enrichment analysis; *MYC*, cellular Myc; *MYCN*, N-Myc; *POU5F1*, *OCT4*; *ALCAM*, *CD166*; *CDH1*, *E-cadherin*; *CDH17*, *Cadherin 17*; *VIM*, *Vimentin*; *SNAI1*, *SNAIL*; *SNAI2*, *SLUG*; *CTSB*, *Cathepsin B*; *MMP2*, *matrix metalloproteinase-2*; SOX2$^+$, high SOX2; CD90$^-$, low CD90 expression; IR, ionizing radiation; EGFR, epidermal growth factor receptor; TIC, tumor initiation cell; SCLC, small cell lung cancer.

Address all correspondence to: Ralph Alexander Schmid, MD, or Thomas Michael Marti, PhD, Division of General Thoracic Surgery, Inselspital, Bern University Hospital, Murtenstrasse 50, 3008 Bern, Switzerland. E-mails: ralph.schmid@insel.ch, thomas.marti@insel.ch

[1] Funding: This work was supported by the Bernese Cancer League and the Swiss Cancer Research (KFS-3530-08-2014) to T. M. M. Research contribution of N. H. was funded by the Carl-Zeiss Foundation (D.4737) and the Bausteinprogramm (LSBN.0103) of the University of Ulm. The funding bodies were not involved in the design of the study; collection, analysis, and interpretation of data; and writing the manuscript.
[2] Contributed equally to this publication.
Received 26 April 2018; Revised 17 September 2018; Accepted 20 September 2018

1476-5586
https://doi.org/10.1016/j.neo.2018.09.008

with an EMT, specifically targeted the otherwise highly resistant paraclone cells. Xenograft tumor formation capacity was 24- and 269-fold higher in holo- than mero- and paraclone cells, respectively. Our results show that A549 subpopulations might serve as a unique system to explore the network of stemness, cellular plasticity, tumor initiation capacity, invasive and metastatic potential, and chemo/radiotherapy resistance.

Neoplasia (2019) 21, 185–196

Introduction

Lung cancer is the most common cause of cancer-related mortality worldwide. More than 80% of lung tumors are non–small cell lung cancers (NSCLCs). A growing body of evidence identified subpopulations of cancer stem cells (CSCs) in various solid tumors that are characterized by an increased expression of stemness-associated genes and drive tumor initiation and therapy resistance (reviewed in [1]). Chemotherapy-resistant subpopulations of cells characterized by CSC marker expression were also identified in lung cancer [2,3]. Interestingly, treatment-resistant lung CSCs displayed an epithelial-to-mesenchymal transition (EMT) phenotype. Indeed, it was proposed that EMT, CSCs, and drug resistance are intrinsically linked (reviewed in [1]).

EMT is a developmental program employed during embryogenesis and in adult organs during wound healing. The activation of this program in cancer cells leads to heritable genetic changes via epigenetic modifications, without the acquisition of new genetic alterations. Upon activation of the program, carcinoma cells shed their epithelial phenotype (e.g., cell-to-cell junctions, polarity, and epithelial marker expression). Instead, they acquire a mesenchymal phenotype, which is associated with therapy resistance and characterized by a fibroblast-like, elongated morphology and an increased migration and invasion capacity (reviewed in [1]). Cisplatin-resistant NSCLC sublines displayed a putative stemness gene signature characterized by increased expression of NANOG, Oct4, and Sox2, which was accompanied by increased expression of CSC markers CD133 and CD44. Interestingly, those cells also featured higher expression of the EMT markers c-Met and Beta-catenin, indicating a hybrid epithelial/mesenchymal (hybrid-E/M) state [4]. The hybrid-E/M state was also described in lung adenocarcinoma cell lines [5].

Primary normal human epidermal cells are heterogeneous in their sustained growth [6]. Single cells give rise to three types of colonies, termed holoclones, meroclones, and paraclones. Holoclones have the greatest reproductive capacity (i.e., extensive proliferation and self-renewal) and, after reseeding, give rise to compact colonies with intact colony borders. Paraclones exclusively contain cells with a short replicative lifespan, which give rise to colonies with wrinkled or disrupted colony borders after reseeding. The meroclone is a transitional stage between the holoclone and paraclone. Holo-, mero-, and paraclones were also described in human cancer cell lines (eg, pancreatic carcinoma [7], glioma, head and neck squamous cell carcinoma, breast and prostate carcinoma cell lines [8–11]). However, whereas the transition from holo- to mero- and paraclone has been described as unidirectional [6], the transition between the different states might not be as restricted in malignant cells. Indeed, phenotypic plasticity has been described *in vitro* in ovarian, breast, and lung cancer cell lines, including plasticity of CD133 expression in the cell line A549 [12–14].

The A549 adenocarcinoma cell line was derived from human carcinomatous lung tissue by Giard et al. [15] and has been widely studied, resulting in more than 19,500 citations in www.pubmed.org to date. Ye et al. [16] identified three types of colonies in the parental A549 cell line, which they described, based on the colony morphology, as holo-, meta-, and paraclones. However, to the best of our knowledge, no report characterizes the distinct cell types composing the parental A549 cell line in detail.

In summary, our study indicates that an untreated *in vitro* culture of the parental cell line A549 is composed of unique subpopulations of cells characterized by distinct features, i.e., tumor initiation capacity, chemotherapy resistance, EMT, and migration/invasion capacity.

Materials and Methods

Full details are provided in *SI Materials and Methods*.

In Vitro Cell Culture and Experiments

Cell lines were cultured as described [17]. Details of the procedure to establish holo-, mero-, and paraclonal subcultures and the *in vitro* experiments are described in *SI Materials and Methods*.

RNA Sequencing and Data Analysis

Illumina paired end sequencing was performed with RNA libraries prepared from three A549 parental cultures plus three subcultures of each type.

Immunofluorescence Microscopy

Cells were seeded at a density of approximately 1 cell/mm^2 and cultured for 6 days. Cells were fixed in paraformaldehyde and subsequently stained for immunofluorescence analysis.

Flow Cytometry

Cells were stained for extracellular markers, fixed, permeabilized, stained for intracellular markers and DNA, and analyzed by flow cytometry.

Animal Experiments and Extreme Limiting Dilution Analysis

Mouse studies were conducted in accordance with Institutional Animal Care and Ethical Committee–approved animal guidelines and protocols.

Immunohistochemical Staining

Tissue was fixed and embedded in paraffin. Immunohistochemical staining was performed using an automated immunostainer.

Methylation Analysis

Genomic DNA was converted by bisulfite treatment; promoter regions of CDH1 and SNAI2 were amplified by PCR and sequenced, allowing the quantitation of methylated CpG sites.

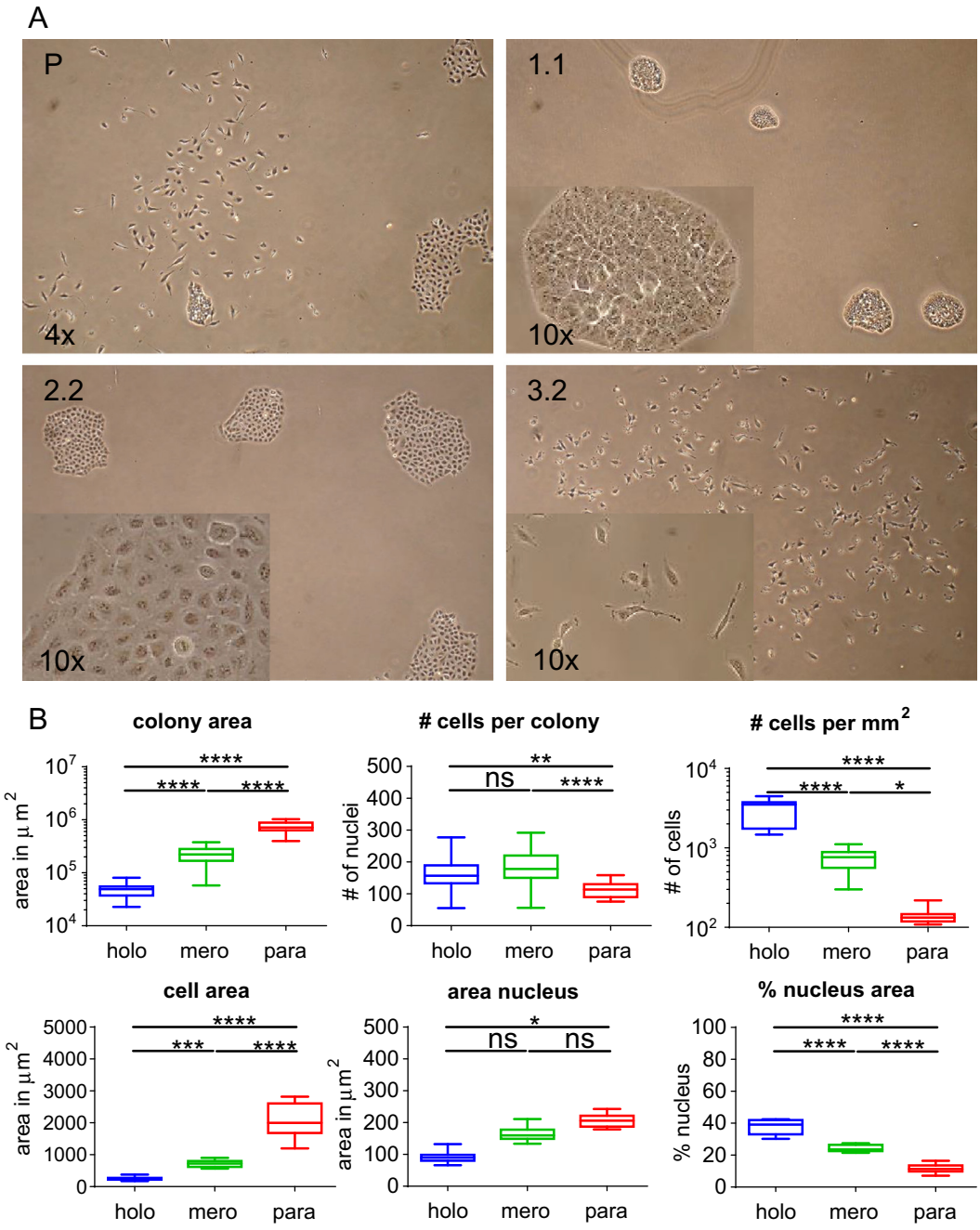

Figure 1. Parental A549 cell cultures contain morphologically distinct cells that give rise to holo-, mero-, and paraclonal colonies. (A) Phase contrast microscopy images of clonal cultures from parental A549 (P), holoclone (1.1), meroclone (2.2), and paraclone cells (3.2). (B) Quantification of area, numbers, and ratios thereof from holo-, mero-, and paraclone cells/colonies by immunofluorescence imaging. All quantifications were made with three individual clonal cultures of holo- (1.1, 1.5, 1.10), mero- (2.2, 2.3, 2.4), and paraclones (3.2, 3.4, 3.7) for which at least 12 colonies ($n = 36$) or 15 cells and nuclei ($n = 45$) were analyzed. Ordinary one-way ANOVA was used for significance analysis (*$P < .05$, **$P < .01$, ***$P < .001$, ****$P < .0001$; n.s., not significant).

Results

Identification of Morphologically Distinct Colonies in the A549 Cell Line

Our previous study indicated that morphologically distinct colonies are identifiable after plating the parental cell line A549 at low density [17]. Indeed, starting from a new aliquot of A549 cells ordered directly from ATCC, phenotypically different colonies were readily identifiable after a few (~3) amplification passages. In detail, phase contrast microscopy revealed three cell and colony morphologies (Figure 1*A*, Parental A549). Based on the published work [6] on cultures of primary human keratinocytes, the clones were termed holo-, mero-, and paraclones. Their frequencies in the parental A549 cell line were 10%, 50%, and 40%, respectively, as we reported [17]. To further characterize these subpopulations, we started from single colonies isolated by cloning rings and removed morphologically diverting colonies over several passages (see the Material and Methods section and Suppl. Figure 1*A*, three distinct subtypes), thereby

establishing clonal cell cultures characterized by a homogenous colony morphology (Figure 1*A* and Suppl. Figure 1*B*).

We detected no differences in cell and colony morphology in the NSCLC cell lines NCI-H460 and NCI-H358. Although we detected colonies with differences in morphology, we could not establish stable long-term cultures of different H2405 subtypes. Six days after seeding, A549 holoclone cells gave rise to round colonies with sharply delineated colony borders and small tightly packed cells (Suppl. Figure 1*C*). In agreement with the initial observation by Barrandon and Green [6], colony borders of meroclones were also continuous but more wrinkled. Finally, paraclones did not have continuous borders and consisted of large, elongated, fibroblast-like cells (Figure 1*A*). Immunofluorescence microscopy confirmed that the average area covered by a holoclone colony was 4 or 16 times less than the average mero- or paraclone colony, respectively (Figure 1*B* and Suppl. Figure 1*D*). The number of cells per colony was marginally but

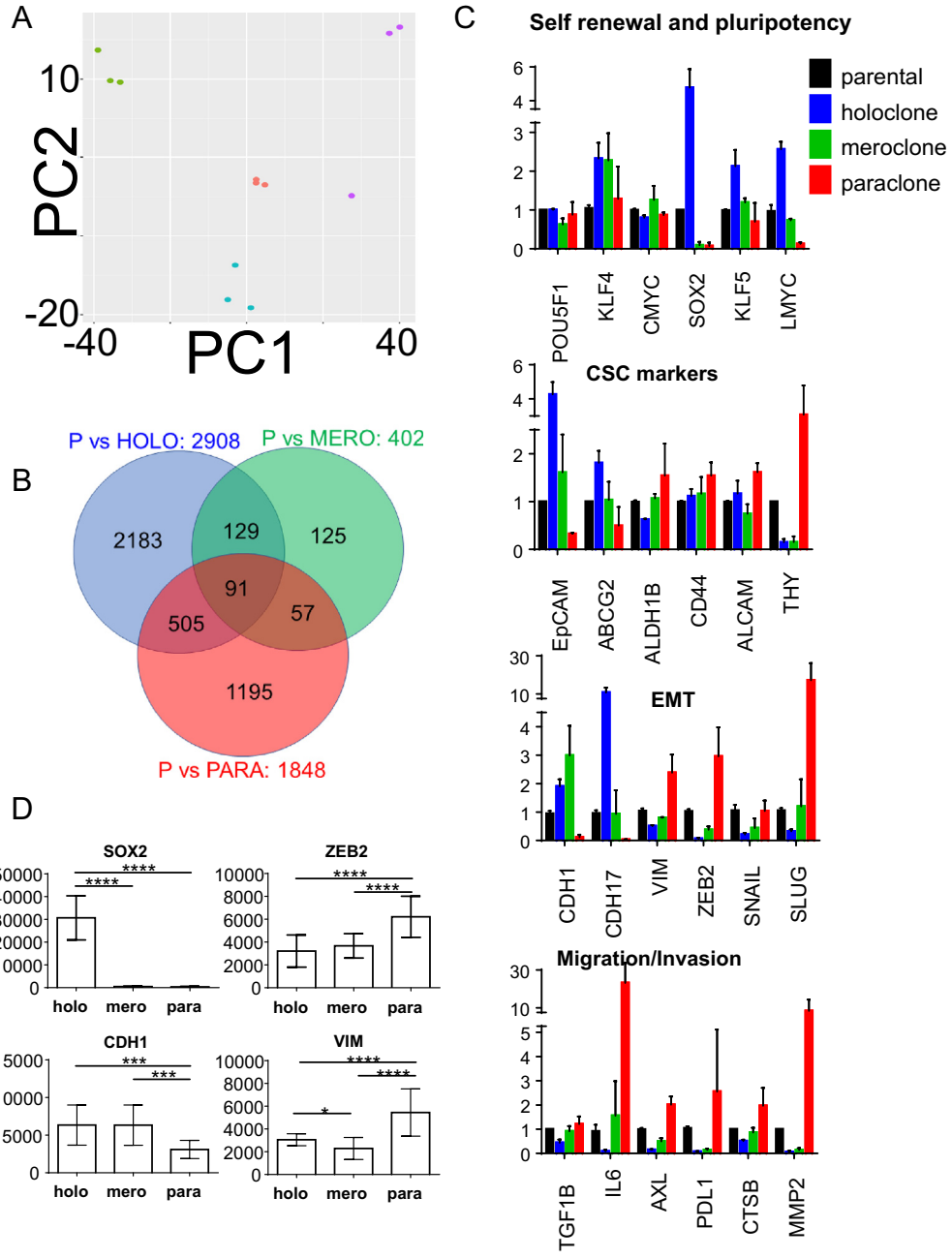

Figure 2. A549 subtypes feature distinct expression patterns. (A) Principal component analysis showing distinct clustering of holoclonal cultures (1.1, 1.2, 1.5) in green, meroclonal cultures (2.2, 2.3, 2.4) in cyan, paraclonal cultures (3.2, 3.4, 3.7) in purple, and the parental cultures in red. PC1: 61% variance, PC2: 15% variance. (B) Venn diagram showing genes that are dysregulated ($P < .05$) in the indicated subtypes compared to parental cells. (C) Expression of selected genes. *Y*-axis represents *X*-fold change of mean ± SD normalized to parental. (D) Quantification of fluorescence signal intensity (minus background) of selected markers detected by immunofluorescence microscopy. *Y*-axis represents mean signal intensity ± SD of three subcultures from holoclone (1.1, 1.5, 1.10), meroclone (2.2, 2.3, 2.4), and paraclone cells (3.2, 3.4, 3.7) ($n = 80$). Ordinary one-way ANOVA was used for significance analysis (*$P < .05$, **$P < .01$, ***$P < .001$, ****$P < .0001$).

significantly lower in paraclones than mero- and holoclones (1.5-fold and 1.33-fold, respectively). Average cell area in paraclones was 2.5-fold and 9-fold larger than in mero- and holoclones, respectively. Differences in nuclear area were less pronounced, resulting in a 3-fold and 1.5-fold smaller ratio of the nuclear versus the total cellular area in para- and meroclones than holoclones, respectively (Figure 1*B*).

Subtypes Are Characterized by Distinct mRNA Expression Profiles

The differences in cell and colony morphology suggest that gene expression is differentially regulated in the three cellular subtypes. To avoid selection bias, we used a genome-wide mRNA expression analysis. Principal component analysis revealed that the subcultures of the same type tightly clustered with each other and there was no overlap with the other subtypes or the parental population (Figure 2*A*).

Expression of 2908, 402, and 1848 genes differed significantly between parental A549 cultures and holo-, mero-, and paraclonal cultures, respectively (Figure 2*B*, adjusted $P > .01$, Suppl. File Tieche RNA-Seq DATA). We used KEGG pathway enrichment analysis (GOseq) to determine the dysregulated biological themes in our dataset (Suppl. File Tieche RNA-Seq DATA/KEGG*). The pathways "ribosome" and "aminoacyl-tRNA biosynthesis," which are both related to protein synthesis, were both significantly dysregulated in the comparison of holo- versus paraclone cells and also in holo- versus meroclone cells, indicating that these pathways are specifically dysregulated in holoclone cells (Suppl. File Tieche RNA-Seq DATA/KEGG*). The majority of remaining pathways specifically dysregulated in holoclone cells were related to metabolism (i.e., galactose metabolism, arginine and proline metabolism, and propanoate metabolism). Paraclone cells were characterized by the dysregulation of pathways involved in cell mobility/migration (i.e., leukocyte transendothelial migration and axon guidance). Remarkably, none of the KEGG pathways was specifically dysregulated in meroclone cells. Indeed, the expression of only 30 and 63 genes was specifically up- or downregulated, respectively, in meroclone cells compared to the two other subtypes (Suppl. File Tieche RNA-Seq DATA/mero*).

Our GOseq analysis indicated that none of the KEGG pathways associated with stemness (e.g., self-renewal and pluripotency) were dysregulated in our subtypes. Conversely, selected genes that are associated with stemness in the context of lung cancer were differentially expressed in our subtypes. In detail, expression of *MYCL* encoding L-MYC, which is amplified and expressed in human small cell lung cancer (SCLC) [18], was 20 times greater in holo- than paraclone cells (Figure 2*C* and Suppl. File Tieche RNA-Seq DATA). However, cellular Myc (*MYC*) and N-Myc (*MYCN*) were not differentially expressed. Similarly, expression of the transcription factors *SOX2* and *KLF5* was 67 and 3.1 times higher in holo- than paraclone cells, respectively, whereas expression of *OCT4 (POU5F1)* and *KLF4* was not dysregulated. Thus, our analysis indicates that the general pathways annotated in the KEGG database are only partially suitable for detecting expression differences in different types of lung cancer cells.

We analyzed expression of selected genes that are specifically associated with lung cancer stem cell markers, EMT, and migration/invasion (Figure 2*C*). *EpCAM* and *ABCG2* are associated with tumor initiation capacity in lung cancer (reviewed in [19]) and were indeed highly overexpressed in holo- compared to paraclone cells. However, the putative lung CSC markers *ALDH1B*, *CD44,* and *CD166 (ALCAM)* [20] were not differentially expressed. Interestingly, *THY1*, also known as *CD90*, which was also described as lung TIC marker [21], was reciprocally expressed compared to other cancer stem cell markers. The epithelial phenotype of holoclone cells was further corroborated by the increased expression of the epithelial markers *E-cadherin* (*CDH1*) and *Cadherin 17* (*CDH17*) and the absence of the mesenchymal markers *THY1* and *Vimentin* (*VIM*) and the mesenchymal transcription factors *ZEB2*, *SNAIL* (*SNAI1*), and *SLUG* (*SNAI2*). Paraclone cells were characterized by a reciprocal expression phenotype (Figure 2*C*).

EMT is associated with migration and invasion (reviewed in [1]). TGF-β and IL-6 induce EMT, and their expression was higher in para- than holoclone cells. The receptor tyrosine kinase AXL induces EMT and regulates the function of breast cancer stem cells [22]. *AXL* expression was 13 times higher in para- than holoclone cells. *Cathepsin B (CTSB)* and *matrix metalloproteinase-2 (MMP2)*, which are involved in extracellular matrix remodeling, were expressed 3.9- and 142-fold less in holo- than paraclone cells, respectively. Interestingly, silencing the expression of the immunomodulator PD-L1 in human gastric cancer cells suppresses not only cell proliferation but also migration and invasion [23]. Indeed, expression of *CD274* encoding PD-L1 was 37-fold increased in para- compared to holoclone cells. Besides PD-L1, multiple targetable immune checkpoint molecules are highly expressed in lung adenocarcinoma characterized by an inflammatory tumor microenvironment, which was highly associated with EMT [24]. Indeed, *PDCD1LG2* encoding PD-L2 was ranked as the 119th most dysregulated gene in holo- compared to paraclone cells, its expression being 235-fold higher in para- than holoclone cells (Suppl. File Tieche RNA-Seq DATA).

In summary, holoclone cells are characterized by an increased expression of epithelial genes and genes associated with lung-specific stemness and cancer stem cell markers. The mRNA expression pattern of paraclone cells is associated with a mesenchymal phenotype. Interestingly, the immunomodulators PD-L1 and PD-L2 are both highly overexpressed in para- versus holoclone cells. Meroclone cells display an intermediate expression phenotype.

Subtypes Have Distinct DNA Methylation Profiles

We next analyzed DNA methylation in the promoter region of *SNAI2* and *CDH1*. Pyrosequencing of bisulfide-converted genomic DNA [25] revealed more methylation in the *CDH1* promoter region of para- than holoclone cells (Suppl. Figure 2*A*). In paraclone cells, methylation levels inversely correlated with mRNA expression of *CDH1,* indicating the functional significance of DNA methylation for transcription regulation of *CDH1*. In the *SNAI2* promoter, no significant subtype-specific methylation differences were detected (Suppl. Figure 2*A*). All subtypes and the parental cell line showed low levels of methylation in the *SNAI2* promoter. These results indicate that DNA methylation is involved in the transcriptional repression of the epithelial marker CDH1 in paraclone cells.

Subtype-Specific Protein Expression of Cell-Surface and Stem-Cell Markers

We extended the characterization of the different cellular subtypes to the protein level. We investigated the localization of differentially expressed proteins by immunofluorescence microscopy. Indeed, nuclear expression of the stemness transcription factor SOX2 and cell surface expression of the epithelial marker CDH1, i.e., E-cadherin, were higher in holo- than paraclone cells. Protein levels of the transcription factor ZEB2 and the cytoplasmic protein

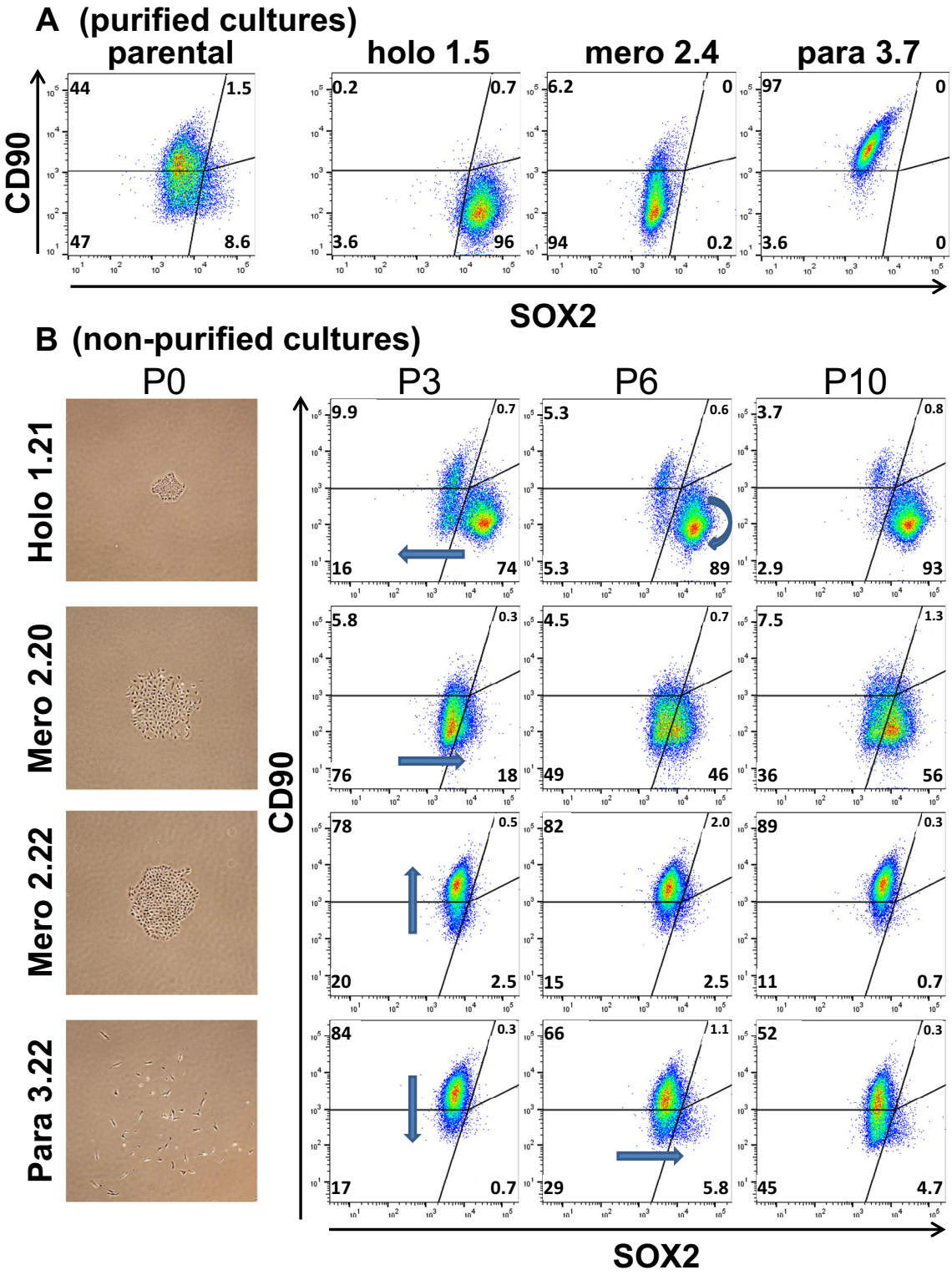

Figure 3. Holo-, mero-, and paraclone cells display phenotypic plasticity over time. (A) Analysis of purified clonal cultures and the parental cell line A549. (B) Analysis of plasticity by flow cytometry over time [e.g., passage 3, 6, and 10 (P3, P6, and P10, respectively)]. Cultures were established from single colonies without the purification procedure. Holo-, mero-, and paraclone cells featured a CD90−/SOX2+, CD90−/SOX2−, and CD90+/SOX2− expression phenotype, respectively. Arrows indicate plasticity trends. P0 shows a phase contrast picture of the original clones used to generate the indicated holo-, mero-, and paraclone subcultures.

VIMENTIN, which are associated with a mesenchymal phenotype, were higher in para- than holoclone cells (Figure 2*D* and Suppl. Figure 2*B*).

In agreement with the gene expression analysis (Figure 2*C*), multicolor flow cytometry analysis of purified cultures revealed that holoclone cells cannot be unambiguously distinguished from

meroclone cells based on EpCAM expression in combination either with SOX2 or with CD90 expression (Suppl. Figure 3*A*). However, holoclone cells can be identified by high SOX2 ($SOX2^+$) and low CD90 expression ($CD90^-$). Paraclone cells are characterized by a reciprocal expression pattern (e.g., $SOX2^-/CD90^+$), whereas the absence of both markers characterizes meroclone cells (e.g., $SOX2^-/CD90^-$) (Figure 3*A*). Within the parental population, our gating strategy revealed that approximately, 50%, 40%, and 10% of cells featured a para-, mero-, and holoclonal expression phenotype, respectively (Figure 3*A*), which is in agreement with our visual quantification [17].

Subtypes Display Phenotypic Plasticity Over Time

During the process of purifying cultures, we observed that morphological homogenous subpopulations frequently give rise to cells and colonies displaying distinctly different morphological features, indicating that the cells can switch from one morphological state to another (Figure 3*B* and Suppl. Figure 1*A*). In other words, individual cells display phenotypic plasticity. We aimed to quantify the observed morphological plasticity by flow cytometry. The expression phenotype of purified cultures from all subtypes remained relatively stable over time (Suppl. Figure 3*B*). We started from single colonies of all three subtypes but omitted the subsequent purification procedure (Figure 3*B*, P0 and Suppl. Figure 3*C*). After three passages of a single holoclonal colony, most cells featured $SOX2^+/CD90^-$ expression, indicating a holoclone phenotype (Figure 3*B*, P3). However, a few cells featured a phenotype characteristic for meroclone or paraclone cells (16% and 10%, respectively). Interestingly, the fraction of mero- and paraclone cells initially detected in nonpurified holoclonal cultures did not increase over time (Figure 3*B*, see also Suppl. Figure 3*C*).

After 6 weeks, cultures that started from nonpurified meroclone cells ($SOX2^-/CD90^-$) displayed phenotypic plasticity towards only one of the other phenotypes [e.g., the meroclone 2.20 showed

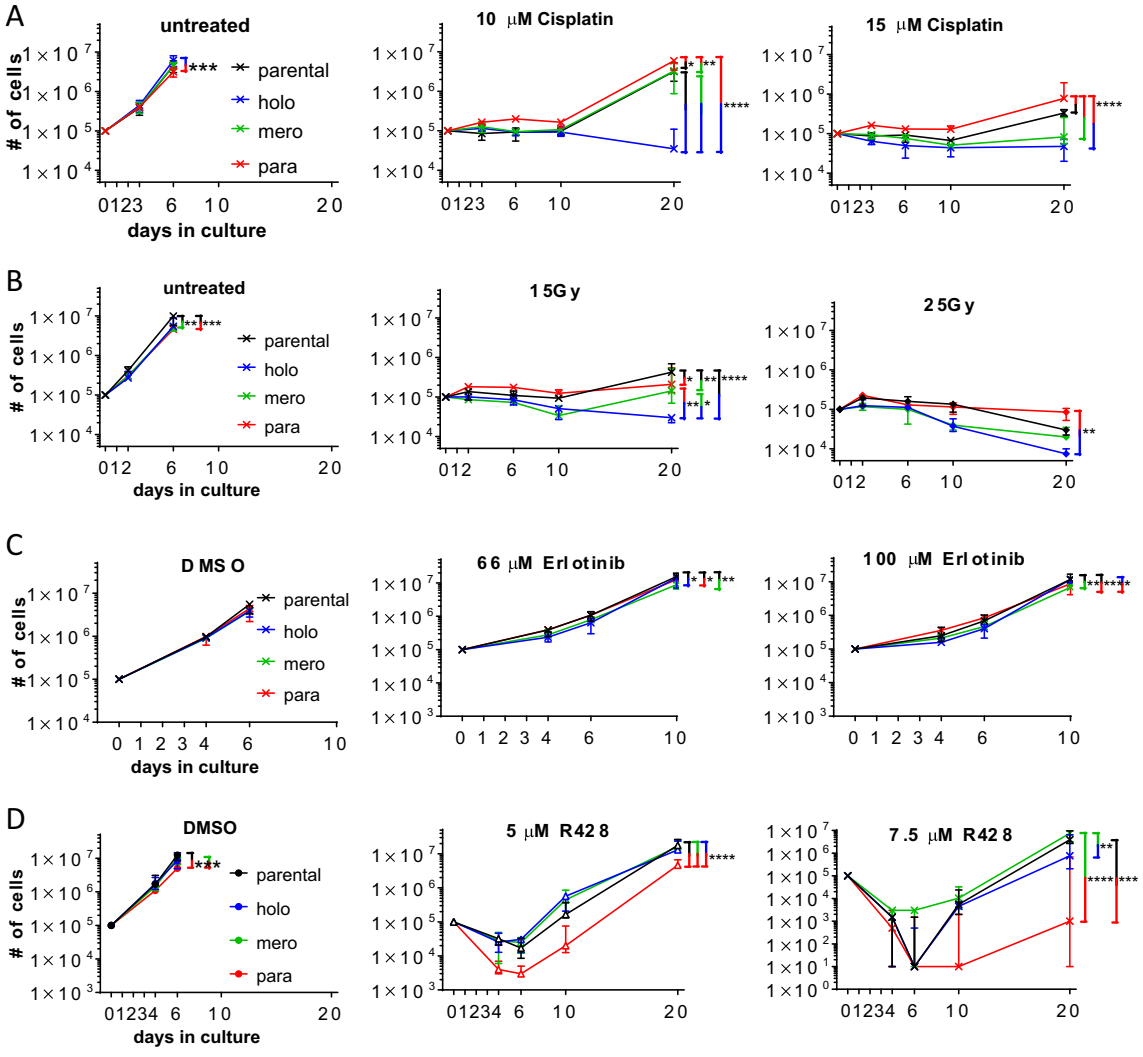

Figure 4. Paraclone cells are resistant to DNA damage induction and EGFR inhibition but most sensitive to AXL inhibition. (A) Cells were treated with cisplatin for 24 hours between days 1 and 2. (B) Cells were exposed to ionizing radiation on day 1. (C) Cells were treated with erlotinib for 72 hours between days 1 and 4. (D) Cells were treated with R428 for 72 hours between day 1 and day 4. Total numbers of live cells were determined over time. Depicted are median and error of three independent experiments done with three parental cultures and three different holo- (1.1, 1.5, 1.10), mero- (2.2, 2.3, 2.4), and paraclone (3.2, 3.4, 3.11) subcultures. Two-way ANOVA was used for significance analysis (*$P < .05$, **$P < .01$, ***$P < .001$, ****$P < .0001$).

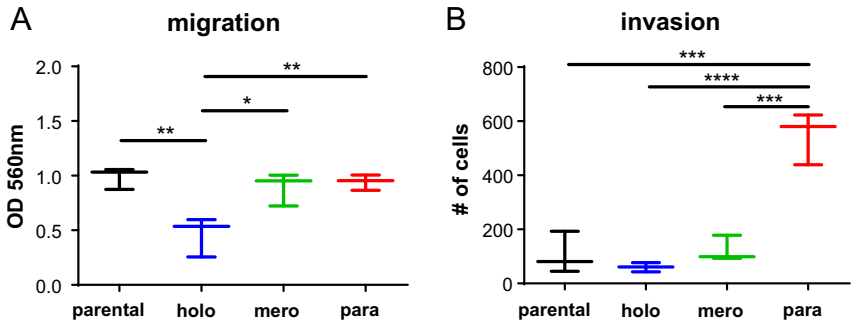

Figure 5. Holo-, mero-, and paraclones display different migratory and invasive potentials. (A) Quantification of migration. (B) Quantification of invasion. The analysis included three subcultures from parental, holoclonal (1.1, 1.5, 1.10), meroclonal (2.2, 2.3, 2.4), and paraclonal (3.2, 3.4, 3.7) cells. Indicated are median and error. Ordinary one-way ANOVA was used for significance analysis (*$P < .05$, **$P < .01$, ***$P < .001$, ****$P < .0001$). Nonsignificant comparisons are not shown.

plasticity toward a holoclonal phenotype, whereas clone 2.22 displayed plasticity toward a paraclonal phenotype (Figure 3*B*, see also Suppl. Figure 3*C* clone 2.21)]. Long-term culture of nonpurified paraclone cells ($SOX2^-/CD90^+$) initially gave rise to another subpopulation featuring a $SOX2^+/CD90^-$ phenotype characteristic of meroclone cells (P3), which over time gave rise to a subpopulation with an expression pattern characteristic for holoclone cells (i.e., $SOX2^+/CD90^-$) (P6/P10).

In summary, holo- and paraclone cells converted to meroclone cells, whereas meroclone cells had the highest phenotypic plasticity, giving rise to subpopulations with a holo- or paraclonal phenotype. Over time, all three subpopulations gave rise to a small fraction of cells that were characterized by concurrent expression of $SOX2^+$ and $CD90^+$, which is characteristic for an E/M-hybrid phenotype (Figure 3*B* and Suppl. Figure 3*C*).

Paraclone Cells Are Resistant to Therapies Inducing DNA Damage

Our experiments revealed that the parental cell line A549 contains cells that feature a CSC-like or a mesenchymal phenotype, but not both. Thus, we evaluated the chemotherapy resistance of the A549 cellular subtypes. During the exponential growth phase (first 6 days after seeding, untreated cultures became confluent), cell growth was similar for the three untreated subtypes compared to parental A549 cells (Figure 4*A*). Treating holoclone cell cultures with 10 μM cisplatin halted cell growth up to 10 days, and cell numbers showed a trend to decrease between day 10 and day 20. In contrast, the other cultures resumed growth at day 10 after treatment with 10 μM cisplatin. Finally, treatment with 15 μM cisplatin halted growth of holo- and meroclonal cultures for up to 20 days. Paraclonal cultures were even more resistant to high-dose (15 μM) cisplatin treatment than the parental cell line (day 20). In agreement, cisplatin treatment selectively reduced the colony formation capacity of holoclone cells compared to parental A549 cells. In contrast, colony formation capacity of paraclone cells was less affected by cisplatin treatment compared to parental A549 cells (Suppl. Figure 4*B*).

Our *in silico* analysis of publicly available retrospective data from primary lung adenocarcinoma patients treated with chemotherapy [26] indicated that high gene expression of the epithelial markers EpCAM, E-cadherin, and Cadherin 17 was associated with significantly longer overall survival. In contrast, mRNA overexpression of the mesenchymal markers CD90, Vimentin, and MMP2 was associated with significantly worse overall survival (Suppl. Figure 4*C*).

To test whether the increased resistance of paraclone cells is specific to cisplatin, we treated stable cultures with ionizing radiation (IR). In contrast to cisplatin treatment, parental cells were most resistant to treatment with 15 Gy IR (Figure 4*B*, see also Suppl. Figure 4*A*). Only after treatment with 25 Gy IR, cell numbers between day 10 and day 20 decreased for the parental cell line, whereas cell numbers did not decrease for cultures of paraclone cells. Cultures of holoclone cells were most sensitive after treatment with 15 and 25 Gy IR, whereas cultures of meroclone cells had an intermediate resistance phenotype.

Paraclone Cells Are Sensitive to AXL Inhibition

To test whether the increased resistance of paraclone cells is specific to therapies inducing DNA damage, we treated stable cultures with erlotinib. Erlotinib is a small-molecule tyrosine kinase inhibitor and is used to treat NSCLC (reviewed in [27]). Expression levels of epidermal growth factor receptor (EGFR), the primary target of Erlotinib, were 2.8-fold higher in para- than holoclone cells, whereas meroclone cells had intermediate expression levels (Suppl. File Tieche RNA-Seq DATA). However, although cultures from all three types were statistically more sensitive to treatment with 100 μM erlotinib than cultures of parental cells, the differences in sensitivity between all the tested cultures were marginal (Figure 4*C*).

Thus, our results indicated that paraclone cells were resistant not only to the tested DNA damage–inducing therapies but also to the inhibition of EGFR signaling. Therefore, we aimed to identify a treatment option that specifically targets these otherwise highly resistant paraclone cells. AXL is a receptor tyrosine kinase whose expression and function are tightly linked with the expression of an EMT signature (reviewed in [1]). *AXL* mRNA expression levels were 13-fold higher in para- compared to holo- and meroclone cells, respectively (Figure 2). siRNA-based silencing of *AXL* blocked A549 subcutaneous tumor growth and increased chemosensitivity [28]. Indeed, cell numbers of all tested cultures were reduced during the initial 72 hours of treatment with the AXL-inhibitor R428 (5 and 7.5 μM) and continued to decrease during the first 3 days of the recovery phase (up to day 6) (Figure 4*D*). During the extended recovery phase (day 10-20), cell growth of all cultures recovered. However, cell numbers of paraclonal cultures were lowest at all tested time points. Thus, paraclone cells proved most sensitive to AXL inhibition. Interestingly, meroclone cells were more resistant to AXL inhibition compared to both holo- and paraclone cells. In summary, paraclone cells were most resistant to DNA damage–inducing treatment regimens but most sensitive to AXL inhibition. Holoclone cells featured a reciprocal resistance phenotype.

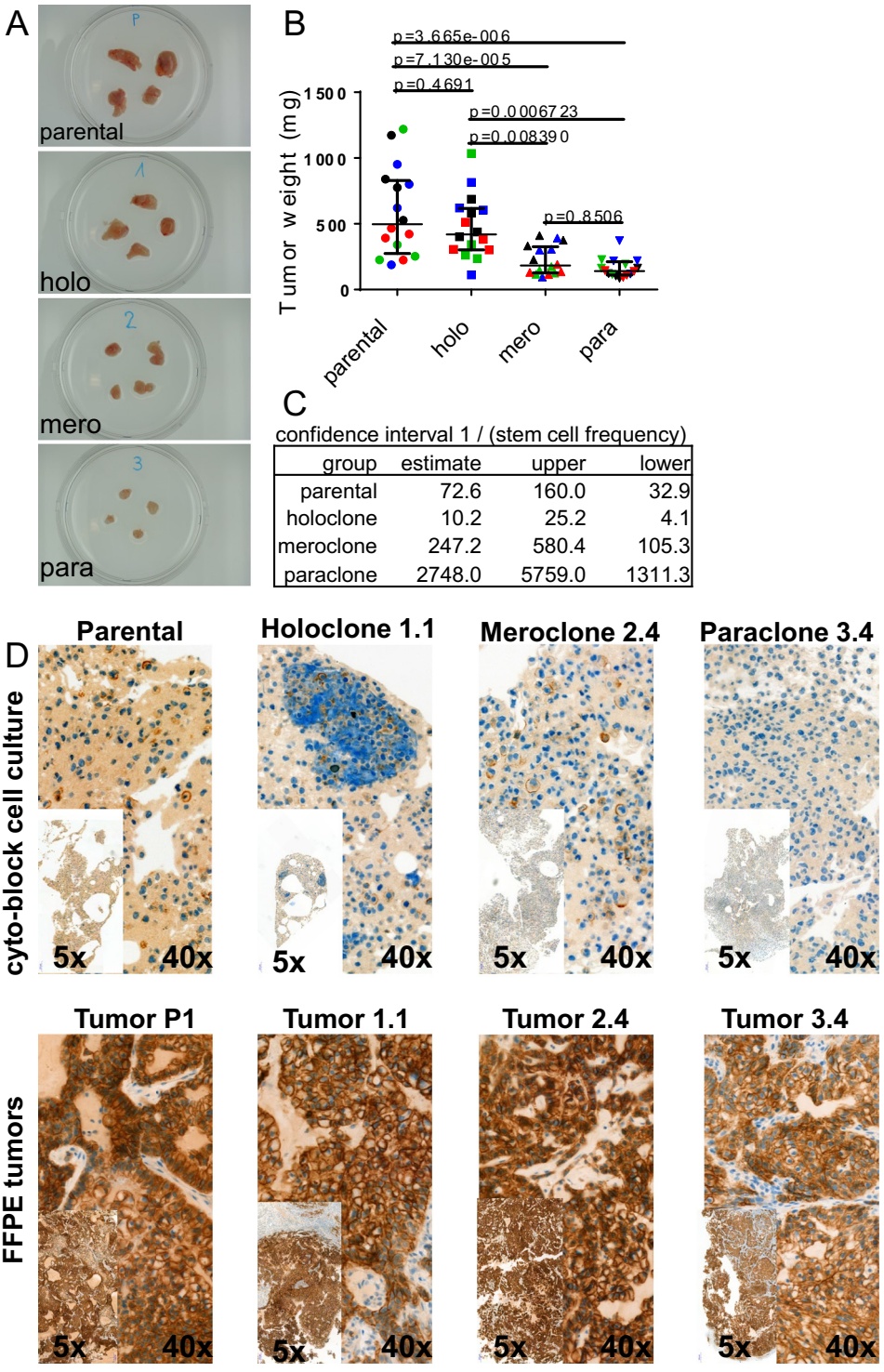

Figure 6. Holoclone cells feature highest tumor growth and tumor initiation capacity. (A) Representative images of tumors explanted 6 weeks after injection of 100,000 cells. (B) Quantification of weight from tumors described above. Depicted are median and interquartile range of four independent experiments (each color represents one experiment) performed with four parental populations and four holoclonal (1.1, 1.2, 1.5, 1.10), three meroclonal (2.2, 2.3, 2.4 P4, 2.4 P8), and four paraclonal (3.2, 3.4, 3.7, 3.9) subcultures. Ordinary one-way ANOVA was used for significance analysis. (C) Tumor-initiating cell frequency was calculated by extreme limiting dilution analysis. (D) Plasticity *in vivo*: acquisition of an epithelial phenotype during tumor growth. Detection of E-cadherin expression by immunohistochemistry.

Invasion Capacity Is Increased in Paraclone Cells

An EMT phenotype is associated with increased migration, invasion, and metastatic capacity (reviewed in [1]). Compared to parental A549 cells, migration capacity was similar in cultures of mero- and paraclone cells but significantly reduced in holoclone cells (Figure 5*A*). The invasion capacity was similar for cultures of parental, holo-, and meroclone cells. Paraclonal cultures featured a significantly increased invasion capacity compared to all other cultures (Figure 5*B*).

In summary, compared to the parental cells, holoclone cells show a reduced migration capacity, whereas paraclone cells feature an increased invasion capacity.

Epithelial-Like Holoclone Cells Feature the Highest Tumor Initiation/Growth Capacity

Lung cancer stem cell marker expression is associated with tumor initiation capacity [2]. Therefore, we determined the tumor growth characteristics of the different A549 subpopulations. Six weeks after subcutaneous cell implantation of 100,000 cells, tumors developed from all subtypes (Figure 6*A*). Implantation of holoclone cells resulted in tumors with a slightly lower average tumor weight compared to the parental cell line, although the difference was not statistically significant (Figure 6*B*). However, the average weight of tumors derived from meroclone cells was significantly lower compared to tumors from holoclone cells and lowest in tumors from paraclone cells.

Since the capacity to initiate tumors might be different from the capacity to support tumor growth, we determined the tumor initiation cell (TIC) frequency by extreme limiting dilution assay. We determined a frequency of 1 TIC per 72.6 parental A549 cells (Figure 6*C* and Suppl. Figure 6). Compared to parental A549 cells, the TIC frequency of holoclone cells was 7.1-fold increased. In contrast, compared to parental cells, the TIC frequency of mero- and paraclone cells was reduced by a factor of 3.4 and 37.9, respectively. In summary, the TIC frequency of holoclone cells was 24.2- and 269-fold higher compared to mero- and paraclone cells, respectively.

Plasticity In Vivo: Acquisition of an Epithelial Phenotype During Tumor Growth

We observed phenotypic plasticity during *in vitro* cultivation of the cellular subtypes; therefore, we investigated whether *in vivo* tumor growth also promotes plasticity. Indeed, cultures of the parental cell line established from xenograft tissue also displayed an increased fraction of meroclone cells (>80%, Suppl. Figure 7) compared to the original *in vitro* culture of parental A549 cells (50%, see [17]). Similarly, compared to the initial purified *in vitro* cultures (purified to ~95%), the fraction of meroclonal colonies after xenotransplantation increased in both holo- and paraclonal cultures (~40% and ~60%, respectively, Suppl. Figure 7). Interestingly, meroclonal cultures remained rather pure during *in vivo* growth (fraction of holoclone and paraclone cells both below 5%, Suppl. Figure 7).

To exclude that the observed plasticity is an *in vitro* cultivation artifact, we also directly stained xenograft tumor tissue by immunohistochemistry (Figure 6*D*). Membranous E-cadherin expression was detectable in control cytoblocks of *in vitro* cultures from parental, holo-, and meroclone cells but absent in blocks from paraclonal cultures. Interestingly, dramatically increased E-cadherin expression was detected in all xenograft tumors.

Discussion

We showed that the untreated parental A549 cell line contains subpopulations characterized by distinct molecular and morphological features. In their seminal study, Barrandon and Green reported that primary cultures of human epidermal cells contain three distinct subpopulations, which feature specific colony-forming potential [6]. Interestingly, holo-, mero-, and paraclones were also found in various human cancer cell lines [7,9,10,29,30]. Morphologically distinct clones were isolated from the cell line A549 by Ye et al. [16]. However, they apparently applied a less stringent definition of the original categories than that proposed by Barrandon and Green [6]. For example, we categorized colonies featuring noncontinuous colony borders as paraclones, whereas such colonies, or at least a fraction of them, were categorized as meroclones by Ye et al. [16]. Ye et al. reported that holoclones gave rise to spheres with a stem cell–like phenotype, which agrees with our findings that holoclones have the most stem-like phenotype.

Andriani et al. recently identified coexisting subpopulations with an epithelial, mesenchymal, or hybrid-E/M phenotype in A549 [31]. However, they reported an epithelial phenotype in 82% of A549 cells, whereas we found even the combined fraction of holo- and meroclone cells to be smaller. These differences might be due to the study-specific *in vitro* culture conditions. Thus, it could be interesting to determine which factor or factors of the growth media determine the frequency of the cellular states within a cell culture. Similarly, it would be interesting to determine how the frequency of the cellular states responds to changes in their growth environment *in vivo*, e.g., determine the distribution of the cellular states not only after subcutaneous (Suppl. Figure 7) but also after orthotopic transplantation.

It has been shown in glioma, head and neck squamous cell carcinoma, and breast and prostate carcinoma cell lines that clones with a tight, intermediate, and loose morphology do exist, i.e., holo-, meso-, and paraclone cells, respectively [8–11]. Thus, the presence of distinct subpopulations is not restricted to A549 or lung cancer cells lines but might be a distinct feature of a subset of cancer cell lines. Subpopulations can be identified in primary cultures of normal cells [6] and might occur in normal cell lines.

Barrandon and Green concluded that the transition of primary keratinocytes from holoclones to meroclone to paraclones is unidirectional and results in progressively restricted growth potential [6]. However, in the context of malignant cells, *in vitro* and *in vivo*, various TIC markers display phenotypic plasticity (i.e., marker-negative cells gain expression of a putative TIC marker over time or vice versa) [12–14,32]. We found that the three cell states can be identified by their differential SOX2 and CD90 mRNA and protein expression levels. Expression of the TIC markers CD133, ALDH, and a side population in A549 cells displays dynamic conversion [14]. We also found a phenotypic plasticity of the three states.

The phenotypic plasticity indicates that the underlying molecular mechanisms guiding the phenotypic changes are reversible. We assume that the changes are not due to genetic alterations since the probability is negligible that spontaneous mutations repetitively give rise to identical phenotypical changes, not to say for the acquisition of an identical, reverting mutation. Regulation of the phenotypic plasticity in the context of EMT is complex and multilayered, with diverse growth factors, micro-RNAs, and epigenetic alterations [5]. We found that DNA methylation is involved in the transcriptional repression of the epithelial marker CDH1 in the paraclone cell clones. Additional studies will be needed to elucidate the network of mechanisms regulating the frequency and the stability of the subpopulations.

Relative to holo- and meroclone cells, paraclone cells were more resistant to chemotherapy and radiation treatment (Figure 4). Interestingly, although the fraction of paraclone cells in the parental cell line was only 45% and thus much lower than in a pure paraclone culture, the parental cell line was most resistant to radiation treatment at lower doses. Similarly, the average weight of tumors established from parental cells was at least as high as those from holoclone cells, although the tumor initiation frequency of holoclone cells was higher

than that of the parental cell line. Interestingly, the tumor initiation capacity of A549 cells is significantly increased by adding mesenchymal stem cells but not by WI38 human lung fibroblasts [33]. Secretion of IL-6 from mesenchymal stem cells enhanced sphere formation and tumor initiation capacity of A549 cells. Indeed, IL-6 gene expression was high in paraclone cells but barely detected in holoclone cells (278-fold difference). Thus, it is tempting to speculate that holoclone cells serve as tumor-initiating cells, whereas paraclone cells provide a mesenchymal niche supporting holoclone cells via paracrine signaling. We found that the immunomodulators PD-L1 and PD-L2 are highly overexpressed in para- versus holoclone cells. More mesenchymal breast carcinoma cells within a tumor retained the ability to protect their more epithelial counterparts from immune attack [34]. Thus, the different clones described here might be an ideal tool to determine if paraclone cells mimic *in vitro* the immunosuppressive function of distinct tumor subpopulations or tumor-associated stroma cells. Additionally, our results confirmed that subpopulations do coexist in a dynamic equilibrium.

It has been proposed that CSCs can be defined by their increased tumor initiation capacity and enhanced therapy resistance, which are both associated with the progression through an EMT (reviewed in [35]. Our results, however, challenge this concept and indicate that the tumor-initiating capacity in lung cancer is associated with an epithelial phenotype and not with a more mesenchymal-like phenotype. In line with our results, chemotherapy-resistant lung adenocarcinoma and leukemia cells are not equivalent to TICs [36]. Further, long-term TICs characterized by high levels of EpCAM and CD24 were identified in a mouse model of SCLC and in human primary SCLC tumors [37]. SCLC TICs were numerous and highly proliferative but not intrinsically chemoresistant, which agree with our data. Thus, for lung adenocarcinoma, to the best of our knowledge, it has so far not been published that chemotherapy resistance and tumor initiation capacity might be specific features of distinct subpopulations.

Our findings lead to a model of the interplay between stemness, chemotherapy resistance, and molecular and phenotypical plasticity in three subpopulations of line A549 (Suppl. Figure 8). We confirmed a fourth subpopulation with concomitant expression of epithelial and mesenchymal markers indicating a hybrid-E/M phenotype, which was described by others [38,39]. In this study, we did not isolate clones with a hybrid-E/M phenotype. Thus, we conclude that the holo-, mero-, and paraclonal states build a plastic tristable system as reported [38]. Jolly et al. postulated that a tristable system is due to the strong mutual inhibition between two transcription factors coupled with strong self-activation of both. In an extension of this model, the hybrid-E/M state most probably represents an additional state with weaker bifurcation points towards the alternative states. Thus, it will be interesting to determine the mechanism underlying this plasticity.

Our model supports the hypothesis that drugs inducing a MET might significantly increase the efficiency of standard chemotherapy (reviewed in [1]). In the context of lung cancer, we showed that kaempferol treatment induced a MET in NSCLC cell lines and primary cultures as indicated by loss of vimentin expression and concomitant induction of E-cadherin expression, which was associated with reversal of MTA resistance [40]. Interestingly, induction of a MET by transduction of reprogramming factors in human squamous cell carcinoma cells reduced metastatic potential and size after xenotransplantation [41]. Thus, induction of a partial MET might decrease chemoresistance but not fully restore tumor initiation capacity. However, a partial MET might induce a hybrid-E/M phenotype, associated with increased tumor initiation capacity and chemotherapy resistance.

Conclusions

Our study suggests that that the parental cell line A549 contains subpopulations characterized by distinct epigenetic states and phenotypical features. The current dogma suggests that cancer stem cells have a stem-like phenotype and are chemoresistant. Thus, our analysis indicates that, at least in lung cancer, the situation might be more complex. Additionally, our protocol for isolating subpopulations from the A549 line might provide a unique system to dissect the molecular network underlying stemness, tumor initiation, therapy resistance, and metastasis in lung cancer.

Declarations

Availability of Data and Materials

All data generated and analyzed during the current study are included in this published article and its supplementary information files.

CRediT authorship contribution statement

Colin Charles Tièche: Conceptualization, Methodology, Data curation, Formal analysis, Writing - original draft. **Yanyun Gao:** Data curation, Formal analysis.
Elias Daniel Bührer: Data curation, Formal analysis, Writing - original draft. **Nina Hobi:** Data curation, Formal analysis.
Sabina Anna Berezowska: Data curation, Formal analysis, Writing - original draft. **Kurt Wyler:** Data curation, Formal analysis.
Laurène Froment: Data curation, Formal analysis. **Stefan Weis:** Data curation, Formal analysis.
Ren-Wang Peng: Data curation, Formal analysis, Writing - original draft. **Rémy Bruggmann:** Formal analysis. **Primo Schär:** Data curation, Formal analysis. **Michael Alex Amrein:** Data curation. **Sean Ralph Robert Hall:** Data curation. **Patrick Dorn:** Formal analysis. **Gregor Kocher:** Formal analysis. **Carsten Riether:** Data curation, Formal analysis. **Adrian Ochsenbein:** Data curation, Formal analysis. **Ralph Alexander Schmid:** Conceptualization, Methodology, Data curation, Formal analysis, Writing - original draft. **Thomas Michael Marti:** Conceptualization, Methodology, Data curation, Formal analysis, Writing - original draft.

Acknowledgements

We thank Dr. José Galván (Institute of Pathology, University of Bern) for technical assistance. Flow cytometry experiments were performed with the support of the FACS Lab at the University of Bern, Switzerland. Microscopy acquisition and analysis were performed with the support of the Live Cell Imaging Core Facility of the Department of Clinical Research coordinated by the Microscopy Imaging Center at the University of Bern, Switzerland. The authors would like to acknowledge Dr. Gary Howard for editing the manuscript concerning the appropriate usage of English.

Appendix A. Supplementary data

Supplementary data to this article can be found online at https://doi.org/10.1016/j.neo.2018.09.008.

References

[1] Shibue T and Weinberg RA (2017). EMT, CSCs, and drug resistance: the mechanistic link and clinical implications. *Nat Rev Clin Oncol* **14**, 611–629.

[2] Eramo A, Lotti F, Sette G, Pilozzi E, Biffoni M, Di Virgilio A, Conticello C, Ruco L, Peschle C, and De Maria R (2008). Identification and expansion of the tumorigenic lung cancer stem cell population. *Cell Death Differ* **15**, 504–514.

[3] Lundholm L, Haag P, Zong D, Juntti T, Mork B, Lewensohn R, and Viktorsson K (2013). Resistance to DNA-damaging treatment in non-small cell lung cancer tumor-initiating cells involves reduced DNA-PK/ATM activation and diminished cell cycle arrest. *Cell Death Dis* **4**, e478.

[4] Barr MP, Gray SG, Hoffmann AC, Hilger RA, Thomale J, O'Flaherty JD, Fennell DA, Richard D, O'Leary JJ, and O'Byrne KJ (2013). Generation and characterisation of cisplatin-resistant non–small cell lung cancer cell lines displaying a stem-like signature. *PLoS One* **8**e54193.

[5] Schliekelman MJ, Taguchi A, Zhu J, Dai X, Rodriguez J, Celiktas M, Zhang Q, Chin A, Wong CH, and Wang H, et al (2015). Molecular portraits of epithelial, mesenchymal, and hybrid States in lung adenocarcinoma and their relevance to survival. *Cancer Res* **75**, 1789–1800.

[6] Barrandon Y and Green H (1987). Three clonal types of keratinocyte with different capacities for multiplication. *Proc Natl Acad Sci U S A* **84**, 2302–2306.

[7] Tan L, Sui X, Deng H, and Ding M (2011). Holoclone forming cells from pancreatic cancer cells enrich tumor initiating cells and represent a novel model for study of cancer stem cells. *PLoS One* **6**e23383.

[8] Cao X, Gu Y, Jiang L, Wang Y, Liu F, Xu Y, Deng J, Nan Y, Zhang L, and Ye J, et al (2013). A new approach to screening cancer stem cells from the U251 human glioma cell line based on cell growth state. *Oncol Rep* **29**, 1013–1018.

[9] Harper LJ, Piper K, Common J, Fortune F, and Mackenzie IC (2007). Stem cell patterns in cell lines derived from head and neck squamous cell carcinoma. *J Oral Pathol Med* **36**, 594–603.

[10] Locke M, Heywood M, Fawell S, and Mackenzie IC (2005). Retention of intrinsic stem cell hierarchies in carcinoma-derived cell lines. *Cancer Res* **65**, 8944–8950.

[11] Li H, Chen X, Calhoun-Davis T, Claypool K, and Tang DG (2008). PC3 human prostate carcinoma cell holoclones contain self-renewing tumor-initiating cells. *Cancer Res* **68**, 1820–1825.

[12] Gunjal P, Pedziwiatr D, Ismail AA, Kakar SS, and Ratajczak MZ (2015). An emerging question about putative cancer stem cells in established cell lines-are they true stem cells or a fluctuating cell phenotype? *J Cancer Stem Cell Res* **3**, e1004. doi:10.14343/JCSCR.2015.3e1004.

[13] Chaffer CL, Brueckmann I, Scheel C, Kaestli AJ, Wiggins PA, Rodrigues LO, Brooks M, Reinhardt F, Su Y, and Polyak K, et al (2011). Normal and neoplastic nonstem cells can spontaneously convert to a stem-like state. *Proc Natl Acad Sci U S A* **108**, 7950–7955.

[14] Akunuru S, James Zhai Q, and Zheng Y (2012). Non-small cell lung cancer stem/progenitor cells are enriched in multiple distinct phenotypic subpopulations and exhibit plasticity. *Cell Death Dis* **3**, e352.

[15] Giard DJ, Aaronson SA, Todaro GJ, Arnstein P, Kersey JH, Dosik H, and Parks WP (1973). In vitro cultivation of human tumors: establishment of cell lines derived from a series of solid tumors. *J Natl Cancer Inst* **51**, 1417–1423.

[16] Ye XQ, Li Q, Wang GH, Sun FF, Huang GJ, Bian XW, Yu SC, and Qian GS (2011). Mitochondrial and energy metabolism-related properties as novel indicators of lung cancer stem cells. *Int J Cancer* **129**, 820–831.

[17] Tieche CC, Peng RW, Dorn P, Froment L, Schmid RA, and Marti TM (2016). Prolonged pemetrexed pretreatment augments persistence of cisplatin-induced DNA damage and eliminates resistant lung cancer stem-like cells associated with EMT. *BMC Cancer* **16**, 125. doi:10.1186/s12885-016-2117-4.

[18] Nau MM, Brooks BJ, Battey J, Sausville E, Gazdar AF, Kirsch IR, McBride OW, Bertness V, Hollis GF, and Minna JD (1985). L-myc, a new myc-related gene amplified and expressed in human small cell lung cancer. *Nature* **318**, 69–73.

[19] Marhaba R, Klingbeil P, Nuebel T, Nazarenko I, Buechler MW, and Zoeller M (2008). CD44 and EpCAM: cancer-initiating cell markers. *Curr Mol Med* **8**, 784–804.

[20] Zhang WC, Shyh-Chang N, Yang H, Rai A, Umashankar S, Ma S, Soh BS, Sun LL, Tai BC, and Nga ME, et al (2012). Glycine decarboxylase activity drives non-small cell lung cancer tumor-initiating cells and tumorigenesis. *Cell* **148**, 259–272.

[21] Yan X, Luo H, Zhou X, Zhu B, Wang Y, and Bian X (2013). Identification of CD90 as a marker for lung cancer stem cells in A549 and H446 cell lines. *Oncol Rep* **30**, 2733–2740.

[22] Asiedu MK, Beauchamp-Perez FD, Ingle JN, Behrens MD, Radisky DC, and Knutson KL (2014). AXL induces epithelial-to-mesenchymal transition and regulates the function of breast cancer stem cells. *Oncogene* **33**, 1316–1324.

[23] Li J, Chen L, Xiong Y, Zheng X, Xie Q, Zhou Q, Shi L, Wu C, Jiang J, and Wang H (2017). Knockdown of PD-L1 in human gastric cancer cells inhibits tumor progression and improves the cytotoxic sensitivity to CIK therapy. *Cell Physiol Biochem* **41**, 907–920.

[24] Lou Y, Diao L, Cuentas ER, Denning WL, Chen L, Fan YH, Byers LA, Wang J, Papadimitrakopoulou VA, and Behrens C, et al (2016). Epithelial-mesenchymal transition is associated with a distinct tumor microenvironment including elevation of inflammatory signals and multiple immune checkpoints in lung adenocarcinoma. *Clin Cancer Res* **22**, 3630–3642.

[25] Bettstetter M, Dechant S, Ruemmele P, Grabowski M, Keller G, Holinski-Feder E, Hartmann A, Hofstaedter F, and Dietmaier W (2007). Distinction of hereditary nonpolyposis colorectal cancer and sporadic microsatellite-unstable colorectal cancer through quantification of MLH1 methylation by real-time PCR. *Clin Cancer Res* **13**, 3221–3228.

[26] Gyorffy B, Surowiak P, Budczies J, and Lanczky A (2013). Online survival analysis software to assess the prognostic value of biomarkers using transcriptomic data in non–small-cell lung cancer. *PLoS One* **8**e82241.

[27] Ciardiello F and Tortora G (2008). EGFR antagonists in cancer treatment. *N Engl J Med* **358**, 1160–1174.

[28] Linger RM, Cohen RA, Cummings CT, Sather S, Migdall-Wilson J, Middleton DH, Lu X, Baron AE, Franklin WA, and Merrick DT, et al (2013). Mer or Axl receptor tyrosine kinase inhibition promotes apoptosis, blocks growth and enhances chemosensitivity of human non–small cell lung cancer. *Oncogene* **32**, 3420–3431.

[29] Liu TJ, Sun BC, Zhao XL, Zhao XM, Sun T, Gu Q, Yao Z, Dong XY, Zhao N, and Liu N (2013). CD133+ cells with cancer stem cell characteristics associates with vasculogenic mimicry in triple-negative breast cancer. *Oncogene* **32**, 544–553.

[30] Beaver CM, Ahmed A, and Masters JR (2014). Clonogenicity: holoclones and meroclones contain stem cells. *PLoS One* **9**e89834.

[31] Andriani F, Bertolini G, Facchinetti F, Baldoli E, Moro M, Casalini P, Caserini R, Milione M, Leone G, and Pelosi G, et al (2016). Conversion to stem-cell state in response to microenvironmental cues is regulated by balance between epithelial and mesenchymal features in lung cancer cells. *Mol Oncol* **10**, 253–271.

[32] Quintana E, Shackleton M, Foster HR, Fullen DR, Sabel MS, Johnson TM, and Morrison SJ (2010). Phenotypic heterogeneity among tumorigenic melanoma cells from patients that is reversible and not hierarchically organized. *Cancer Cell* **18**, 510–523.

[33] Hsu HS, Lin JH, Hsu TW, Su K, Wang CW, Yang KY, Chiou SH, and Hung SC (2012). Mesenchymal stem cells enhance lung cancer initiation through activation of IL-6/JAK2/STAT3 pathway. *Lung Cancer* **75**, 167–177.

[34] Dongre A, Rashidian M, Reinhardt F, Bagnato A, Keckesova Z, Ploegh HL, and Weinberg RA (2017). Epithelial-to-mesenchymal transition contributes to immunosuppression in breast carcinomas. *Cancer Res* **77**, 3982–3989.

[35] Pattabiraman DR and Weinberg RA (2014). Tackling the cancer stem cells — what challenges do they pose? *Nat Rev Drug Discov* **13**, 497–512.

[36] Hegde GV, de la Cruz C, Eastham-Anderson J, Zheng Y, Sweet-Cordero EA, and Jackson EL (2012). Residual tumor cells that drive disease relapse after chemotherapy do not have enhanced tumor initiating capacity. *PLoS One* **7**e45647.

[37] Jahchan NS, Lim JS, Bola B, Morris K, Seitz G, Tran KQ, Xu L, Trapani F, Morrow CJ, and Cristea S, et al (2016). Identification and targeting of long-term tumor-propagating cells in small cell lung cancer. *Cell Rep* **16**, 644–656.

[38] Jolly MK, Boareto M, Huang B, Jia D, Lu M, Ben-Jacob E, Onuchic JN, and Levine H (2015). Implications of the hybrid epithelial/mesenchymal phenotype in metastasis. *Front Oncol* **5**, 155 (https://www.ncbi.nlm.nih.gov/pubmed/26258068).

[39] Jolly MK, Tripathi SC, Jia D, Mooney SM, Celiktas M, Hanash SM, Mani SA, Pienta KJ, Ben-Jacob E, and Levine H (2016). Stability of the hybrid epithelial/mesenchymal phenotype. *Oncotarget* **7**, 27067–27084.

[40] Liang SQ, Marti TM, Dorn P, Froment L, Hall SR, Berezowska S, Kocher G, Schmid RA, and Peng RW (2015). Blocking the epithelial-to-mesenchymal transition pathway abrogates resistance to anti-folate chemotherapy in lung cancer. *Cell Death Dis* **6**, e1824.

[41] Takaishi M, Tarutani M, Takeda J, and Sano S (2016). Mesenchymal to epithelial transition induced by reprogramming factors attenuates the malignancy of cancer cells. *PLoS One* **11**e0156904.